Differences in Mitochondrial Coupling Reveal a Novel Signature of Mitohormesis in Muscle of Healthy Individuals

Lauren M. Sparks, Leanne M. Redman, Kevin E. Conley, Mary-Ellen Harper, Andrew Hodges, Alexey Eroshkin, Sheila R. Costford, Meghan E. Gabriel, Fanchao Yi, Cherie Shook, Heather H. Cornnell, Eric Ravussin, and Steven R. Smith*

Context: Reduced mitochondrial coupling (ATP/O_2 [P/O]) is associated with sedentariness and insulin resistance. Interpreting the physiological relevance of P/O measured in vitro is challenging.

Objective: To evaluate muscle mitochondrial function and associated transcriptional profiles in nonobese healthy individuals distinguished by their in vivo P/O.

Design: Individuals from an ancillary study of Comprehensive Assessment of Long-term Effects of Reducing Intake of Energy phase 2 were assessed at baseline.

Setting: The study was performed at Pennington Biomedical Research Center.

Participants: Forty-seven (18 males, 26–50 y of age) sedentary, healthy nonobese individuals were divided into 2 groups based on their in vivo P/O.

Intervention: None.

Main Outcome(s): Body composition by dual-energy x-ray absorptiometry, in vivo mitochondrial function (P/O and maximal ATP synthetic capacity) by ^{31}P-magnetic resonance spectroscopy and optical spectroscopy were measured. A muscle biopsy was performed to measure fiber type, transcriptional profiling (microarray), and protein expressions.

Results: No differences in body composition, peak aerobic capacity, type I fiber content, or mitochondrial DNA copy number were observed between the 2 groups. Compared with the uncoupled group (lower P/O), the coupled group (higher P/O) had higher rates of maximal ATP synthetic capacity (maximal ATP synthetic capacity, $P < .01$). Transcriptomics analyses revealed higher expressions of genes involved in mitochondrial remodeling and the oxidative stress response in the coupled group. A trend for higher mitonuclear protein imbalance ($P = .06$) and an elevated mitochondrial unfolded protein response (heat shock protein 60 protein; $P = .004$) were also identified in the coupled group.

Conclusions: Higher muscle mitochondrial coupling is accompanied by an overall elevation in mitochondrial function, a novel transcriptional signature of oxidative stress and mitochondrial remodeling and indications of an mitochondrial unfolded protein response. **(*J Clin Endocrinol Metab* 101: 4994–5003, 2016)**

ISSN Print 0021-972X ISSN Online 1945-7197
Printed in USA

Received July 19, 2016. Accepted October 3, 2016.
First Published Online October 6, 2016

* Author Affiliations are shown at the bottom of the next page.

Abbreviations: ANT, adenine nucleotide translocase; ATPflux, ATP turnover; ATPmax, ATP synthetic capacity; CALERIE, Comprehensive Assessment of Long term Effects of Reducing Intake of Energy; *CPEB2*, cytoplasmic polyadenylation element-binding protein 2; CR, caloric restriction; *CS*, citrate synthase; CV, coefficient of variation; ETS, electron transport system; GSEA, gene set enrichment analysis; 4-HNE, 4-hydroxy-2-nonenal; HSP, heat shock protein; IMCL, intramyocellular lipid; MRS, magnetic resonance spectroscopy; mtDNA, mitochondrial DNA; NAD, nicotinamide adenine dinucleotide; *NAMPT*, nicotinamide phosphoribosyltransferase; nDNA, nuclear DNA; P/O, ATP/O_2; *PPARD*, peroxisome proliferator-activated receptor-δ; *PPARGC1A*, peroxisome proliferator-activated receptor-γ coactivator 1α; qRT-PCR, quantitative RT-PCR; ROS, reactive oxygen species; TCA, tricarboxylic acid; UCP, uncoupling protein; UPR^{mt}, mitochondrial unfolded protein response; VL, vastus lateralis; VO_2peak, peak aerobic capacity.

Sedentariness and insulin resistance are associated with reduced muscle mitochondrial coupling, which is improved with endurance training (1). We recently demonstrated in vivo that athletes have elevated muscle mitochondrial coupling, accompanied by high rates of ATP synthesis and antioxidant enzyme content, compared with lean sedentary individuals (2). High oxidative capacity and elevated mitochondrial coupling generate reactive oxygen species (ROS) and potentially deleterious by-products, such as hydrogen peroxide and 4-hydroxy-2-nonenal (4-HNE) (3), suggesting that an effective oxidative stress response may serve as a buffer for ROS production. The underlying mechanism(s) responsible for this phenomenon are poorly understood. Studies in rats selectively bred for high-capacity running have shown that high rates of muscle oxidative phosphorylation are associated with high rates of ROS production and elevation in the antioxidant enzyme superoxide dismutase 2 (4). The authors concluded that greater capacity of high-capacity running muscle for work and hydrogen peroxide signaling resulted in enhanced and more immediate cellular repair, possibly explaining the lower disease risks seen in these animals (4). A positive feedback loop whereby elevated phosphorylating respiration elicits an oxidative stress response and subsequent increased antioxidant capacity through ROS generation is a plausible explanation for parallel elevations in mitochondrial function and oxidative stressin a healthy phenotype.

The interaction between mitochondrial coupling (ATP/O_2 [P/O]) and oxidative stress clearly plays a significant role in controlling cellular health. The capacity of mitochondria to oscillate between an uncoupled and coupled state potentially determines its ability to protect against deleterious effects of high levels of ROS. Assessing this interplay in vitro is challenged by the lack of physiological concentrations of substrates (eg, fatty acids [FAs]) and purine nucleotides (eg, GDP) known to have effects on (un)coupling (5, 6). Pairing noninvasive in vivo ^{31}P-magnetic resonance spectroscopy (MRS) with optical spectroscopy is an advantageous approach to studying P/O. We demonstrate that in nonobese healthy humans, higher muscle P/O is associated with elevated maximal ATP synthesis and expressions of genes related to mitochondrial function, particularly those involved in nicotinamide adenine dinucleotide $(NAD)^+$ biosynthesis, the oxidative stress response, and mitochondrial remodeling (fusion/fission).

Materials and Methods

Participants

Forty-seven (18 males) healthy, young- and middle-aged (26–50 y) nonobese (body mass index, 21.5 to 28.4 kg/m^2) enrolled in the Comprehensive Assessment of Long-term Effects of Reducing Intake of Energy (CALERIE) phase 2 trial at Pennington Biomedical Research Center, elected to participate in this ancillary in which they underwent multinuclear MRS (^{1}H and ^{31}P) and optical spectroscopy measurements of skeletal muscle and a muscle biopsy at baseline, before randomization. The design and rationale of CALERIE has been described previously (7). The study was approved by the Institutional Review Board of the Pennington Biomedical Research Center and conformed to the Declaration of Helsinki. Participants gave written informed consent.

Blood analyses

Venous blood samples were obtained after fasting overnight and analyzed in a central laboratory.

Peak aerobic capacity (VO_2peak)

VO_2peak was measured using the Cornell incremental treadmill test as previously described (8).

Body composition

Body composition was obtained by dual-energy x-ray absorptiometry scan (QDA 4500A; Hologics) and analyzed as previously described (8).

MRS and optical spectroscopy

MRS was performed on a 3T GE Signa Excite (General Electric).

In vivo intramyocellular lipid (IMCL)

IMCL content of the soleus and tibialis anterior muscles was measured by ^{1}H-MRS using the PRESS technique (9). Briefly, $1 \times 1 \times 1$-cm voxels were placed within the muscle, and spectra were acquired for approximately 4 minutes. Peak positions and areas of interest were determined by time domain fitting using jMRUI. Areas of interest were expressed in arbitrary units per voxel area relative to internal water (%IMCL = IMCL peak area/water peak area $\times$ 100).

Coefficient of variation (CV) for IMCL is $\pm$6.3% (see reference 19 below).

In vivo mitochondrial function (O_2 uptake, ATP turnover [ATPflux], maximal ATP synthetic capacity [ATPmax], and P/O)

Resting O_2 uptake was measured in the vastus lateralis (VL) muscle by optical spectroscopy (Horiba Jobin Yvon) (10). The CV for O_2 uptake is $\pm$13.7%.

Translational Research Institute for Metabolism and Diabetes (L.M.S., F.Y., C.S., H.H.C., S.R.S.), Florida Hospital, Orlando, Florida 32804; Clinical and Molecular Origins of Disease (L.M.S., M.E.G., S.R.S.), Sanford Burnham Prebys Medical Discovery Institute, Orlando, Florida 32827; Pennington Biomedical Research Center (L.M.R., E.R.), Louisiana State University System, Baton Rouge, Louisiana 70808; Departments of Radiology, Physiology and Biophysics, and Bioengineering (K.E.C.), University of Washington Medical Center, Seattle, Washington 98195; Department of Biochemistry, Microbiology, and Immunology (M.-E.H.), University of Ottawa, Ottawa, Ontario ON K1N 6N5, Canada; Bioinformatics Core (A.H., A.E.), Sanford Burnham Prebys Medical Discovery Institute, La Jolla, California 92037; and Hospital for Sick Children (S.R.C.), Toronto, Ontario, ON M5G 1X8 Canada

ATPflux and ATPmax were measured in the VL by ^{31}P-MRS as previously described (11). The CVs are is ±11.0% and ±9.0%, respectively.

Mitochondrial coupling was calculated as the ratio of ATPflux to O_2 uptake and was divided by 2 to yield P/O (ie, number of ATPs produced per pair of electrons traveling through the electron transport system [ETS]). The CV is ±6% (2).

Muscle biopsy, fiber type, and IMCL

A muscle biopsy was performed at the same site as the ^{31}P and optical spectroscopy measurements using the Bergstrom technique (12). Fiber type and IMCL contents of the VL were quantified by immunohistochemistry as previously described (13).

DNA isolation and mitochondrial content

Total DNA was isolated from approximately 10 mg of skeletal muscle tissue using the DNeasy kit (QIAGEN) and relative amounts of mitochondrial DNA (mtDNA) and nuclear DNA (nDNA) were determined by real-time quantitative PCR as previously described (14).

RNA isolation and real-time quantitative RT-PCR (qRT-PCR)

Total RNA was isolated from approximately 20 mg of skeletal muscle tissue using the RNeasy Fibrous Tissue kit (QIAGEN). Primer-probe sets were predesigned Single Tube Taqman Gene expression assays. qRT-PCR reactions were performed using Taqman Fast Virus 1-step reaction mix Standard protocol (Life Technologies). Data were normalized by dividing the target gene by the geometric mean of the internal control genes (*RPLP0*, *GAPDH*, and *PPIB*).

Transcriptomics

Near-whole-genome transcriptome analysis was performed using the Illumina bead-based technology and Sentrix Human-6 V2 Expression BeadChip (Illumina, Inc). Illumina data were initially log2 normalized and batch corrected using Partek software (15). Mutual information was computed using the AracNe algorithm (16) on a next-gen server to identify all possible transcriptional interactions inferred based on the processed dataset. This algorithm was repeated using different *P* value cutoffs ($P <$ 1E-2, $P <$ 1E-5, and $P <$ 1E-7). The number of inferred interactions which met each selected cutoffs varied (5.0E5, 2.6E4, and 1.4E3, respectively), thus providing different interactomes with varying levels of support (with the most stringent *P* values providing the best-supported interactions). Multiple *P* value cutoffs were used to generate separate "interactomes" for the later Viper analysis (17). Next, a paired Student's *t* test was applied in R following the Viper protocol on Bioconductor with 1000 null ("dnull") distributions computed for further comparison. Finally, the "msviper" command was executed using a selected mutual information interactome from AracNe, the signature computed from the paired *t* test and the dnull null distribution. Viper regulons were then prioritized according to the viper *P* value metric and absolute value of normalized enrichment scores. The results were loaded into our Regulattice (http://regulattice.sbpdiscovery.org) website for score comparison and interactive network visualizations using D3.js. Key comparisons were matched against the known mitochondrial gene/protein identifiers from MitoCarta 2.0 (18).

Gene set enrichment analysis (GSEA) (19) was run in GenePattern (20) using either the Hallmarks ("H.all.v5.1.symbols.gmt") or Reactome ("c2.cp.reactome.v5.symbols.gmt") gene sets from GSEA and mSigDB (21). Significant pathways and enriched categories with $P < .05$ were identified and analyzed.

Western blotting

Western blotting was quantified using the Odyssey infrared imaging system (LI-COR Biosciences) for the following antibodies: heat shock protein (HSP)60 (1:1000, sc-1052; Santa Cruz Biotechnology) and IRDye 680RD Donkey antigoat IgG (1: 15 000, 925-68074; LI-COR Biosciences). Protein adducts of 4-HNE were determined as a marker of lipid peroxidation using a polyclonal anti-4-HNE antibody (Calbiochem). Sample normalization was conducted according to manufacturer's protocol using the LI-COR Biosciences REVERT Total Protein Stain.

Statistical analysis

Analyses were performed using JMP version 12 (SAS Institute) unless otherwise indicated. Variables were preexamined for normal distribution. Gender distribution was analyzed by χ^2 test. For comparisons of group means, unpaired Student's *t* tests were used. Based on the distribution of in vivo mitochondrial coupling (P/O), the cohort of 47 nonobese healthy individuals was divided into 2 groups according to a median split (P/O = 1.22). Data in Figure 2 below are expressed as the relative differences of the coupled group over the uncoupled (set to 1). SEM was calculated using error propagation equations derived from the Gaussian equation for normally distributed errors. Data are expressed as mean ± SEM. Level of significance was set at $P <$ .05. Clinical trials registration numbers are NCT00427193 and NCT02695511.

Results

Higher in vivo mitochondrial coupling is reflective of mitochondrial function not content

Pairing noninvasive in vivo ^{31}P-MRS with optical spectroscopy is an advantageous approach to studying mitochondrial coupling (P/O). Based on the distribution of in vivo P/O, we divided a cohort of 47 nonobese healthy individuals into 2 groups according to a median split of their P/O. The "uncoupled" group had significantly lower resting ATPflux ($P <$ .001) (Figure 1A) and significantly higher O_2 uptake ($P <$ .01) (Figure 1B) with a resulting P/O significantly lower than the "coupled" group ($P <$ .001) (Figure 1C). The uncoupled group had a P/O < 1.22, and the coupled group had a P/O ≥ 1.22. For the entire cohort, P/O ranged from 0.49 to 2.17. With the exception of high-density lipoprotein being higher in individuals with higher P/O ($P <$ .05) (Table 1), no significant differences were observed between the groups in terms of age, weight, body composition, and serum metabolic profiles (Table 1).

ATPmax was approximately 28% higher in individuals with higher P/O (coupled vs uncoupled; $P = .003$) (Figure 1D). Because we found no differences in VO_2peak be-

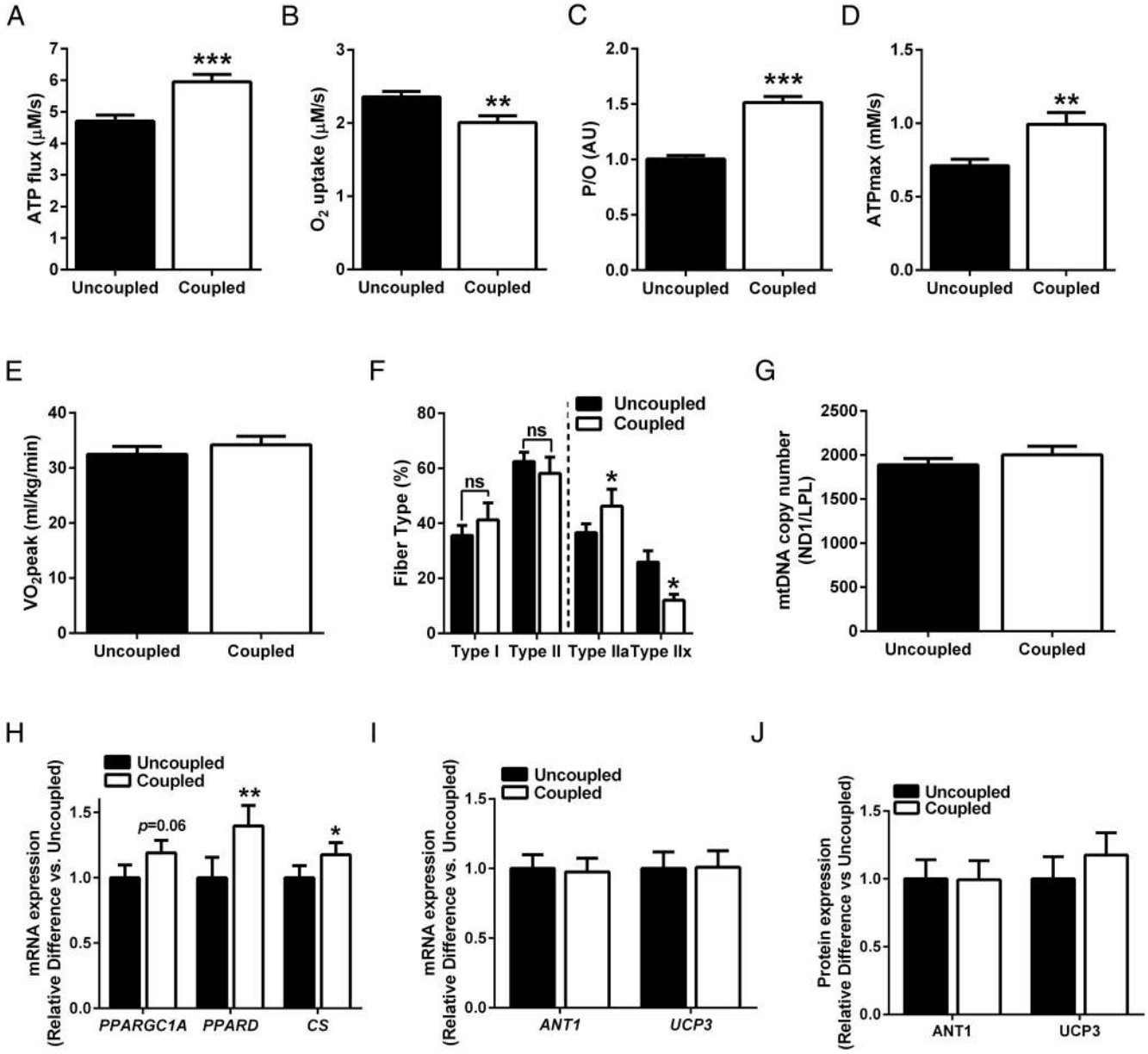

Figure 1. Higher in vivo muscle mitochondrial coupling is not related with aerobic capacity, fiber type, or mitochondrial content. Resting ATP flux (A), O_2 uptake (B), ATP flux/O_2 uptake or P/O (C), and maximal ATP synthetic rates (ATPmax) (D) were measured by ^{31}P-MRS and optical spectroscopy in a cohort of healthy nonobese individuals separated by their in vivo mitochondrial coupling (P/O). VO_2peak was measured during an incremental treadmill test (E) and muscle fiber type composition by immunohistochemistry (F). mtDNA copy number was assessed by quantitative PCR (qPCR) (G). mRNA expressions were measured by qRT-PCR and protein contents were assessed by Western blotting (H–J) and are expressed as the relative difference of the coupled group over the uncoupled (which was set to 1). P/O, in vivo muscle mitochondrial coupling; uncoupled group (P/O $<$ 1.22); coupled group (P/O $\geq$ 1.22); NS, not significant. Black bars indicate uncoupled and white bars indicate coupled. Due to unforeseen instrument acquisition failures, not all participants have spectroscopy data. For ATP flux, O_2 uptake and P/O, n = 24 (uncoupled) and n = 23 (coupled); for ATPmax, n = 22 (uncoupled) and n = 21 (coupled); for VO_2peak, n = 24 (uncoupled) and n = 23 (coupled). Due to limited tissue availability, not all participants have biopsy-derived data. For fiber type, n = 13 (uncoupled) and n = 9 (coupled); mtDNA, mRNA and protein, n = 16 (uncoupled) and n = 15 (coupled). ***, $P < .001$; **, $P < .01$; *, $P < .05$.

tween the groups ($P = .41$) (Figure 1E), we hypothesized that the coupled group was more physically active despite similar VO_2peak. Energy expenditure associated with spontaneous physical activity during a 24-hour stay in the metabolic chamber, however, did not differ between groups ($P = .21$) (data not shown).

We speculated that differences in fiber type composition might be related with the differences in P/O. However, no differences in % of type I or II fibers were observed between the groups (type I: 41.2% vs 35.6%, $P = .35$ and type II: 58.2% vs 62.4%, $P = .53$; coupled vs uncoupled, respectively) (Figure 1F). Composition of type II fibers, however, did differ between groups. Type IIa fibers were 21% higher ($P = .05$) and type IIx fibers were 54% lower ($P = .02$) in the coupled vs the uncoupled group (Figure 1F). Mitochondrial content (mtDNA

Table 1. Clinical Characteristics

Clinical Variable	Uncoupled Group	Coupled Group	*P* Value
Age (y)	38.1 ± 6.6	41.1 ± 5.8	NS
Sex (M/F)	8/16	10/13	NS
Weight (kg)	71.1 ± 9.9	73.4 ± 8.4	NS
Body mass index (kg/m^2)	25.0 ± 1.6	25.3 ± 1.9	NS
Body fat (%)	32.3 ± 5.2	32.1 ± 7.3	NS
Fat mass (kg)	22.7 ± 3.8	23.4 ± 5.0	NS
Fat-free mass (kg)	48.3 ± 9.3	50.0 ± 9.5	NS
Glucose (mg/dL)	83.3 ± 4.8 (4.6 ± 0.3)	81.5 ± 6.2 (4.5 ± 0.3)	NS
Cholesterol (mg/dL)	162.4 ± 34.8 (4.2 ± 0.9)	175.7 ± 25.7 (4.6 ± 0.7)	NS
HDL (mg/dL)	43.2 ± 8.1 (1.1 ± 0.2)	52.0 ± 14.7 (1.3 ± 0.4)	<.05
LDL (mg/dL)	100.5 ± 28.1 (2.6 ± 0.7)	103.2 ± 19.2 (2.7 ± 0.5)	NS

Data are mean ± SD. P/O, in vivo muscle mitochondrial coupling; uncoupled group (P/O < 1.22); coupled group (P/O ≥ 1.22). All blood variables were obtained during the fasted state. NS, not significant. HDL, high-density lipoprotein; LDL, low-density lipoprotein. Where applicable, SI units are in parentheses to indicate mmol/L.

copy number) did not differ between groups ($P = .36$) (Figure 1G).

To further understand the observed link between in vivo P/O and ATPmax, we measured mRNA expressions of key markers of oxidative metabolism and tricarboxylic acid (TCA) cycle genes (peroxisome proliferator-activated receptor-γ coactivator 1α [*PPARGC1A*], peroxisome proliferator-activated receptor-δ [*PPARD*], and citrate synthase [*CS*]). We found that they were elevated in the coupled vs the uncoupled group (Figure 1H), suggestive of enhanced mitochondrial capacity. Given that the uncoupled group had P/O values less than 1.22, indicating mild uncoupling, we anticipated differences in uncoupling proteins (UCPs) between the 2 groups.UCP3 and adenine nucleotide translocase (ANT)1 were not different between groups either at a transcript or a protein level (Figure 1, I and J). Posttranslational modifications of UCP3 (22) and ANT1 proteins (23) play a significant role in the function of the protein itself. As such, differences in uncoupling activity cannot be ruled out.

The oxidative stress response and mitochondrial remodeling associate with a more coupled phenotype

Hypothesizing that the transcriptional profile would be related with in vivo P/O, we performed an unsupervised microarray analysis of the muscle tissue in a representative subset of individuals (n = 9 per group). The heat map in Figure 2A demonstrates the reciprocal expression patterns of genes differentially regulated between the 2 groups. Initial enrichment analyses revealed gene ontology processes related to oxidative stress and apoptosis (False Discovery Rate < 0.01 for all) (data not shown). A more in-depth bioinformatics analysis (Viper) (17) revealed a novel master regulator, cytoplasmic polyadenylation element-binding protein 2 (*CPEB2*), which had a predicted 1005 interactions with differentially expressed genes (Figure 2B). *CPEB2*, which plays a critical role in the immediate response to oxidative stress as a negative regulator of hypoxia-inducible factor 1α (*Hif1a*) translation (24), was significantly reduced ($P = .002$, False Discovery Rate = 0.007) (Figure 2B) in the coupled vs uncoupled group. We found that 4% of these 1005 genes regulated by *CPEB2* (regulon members) were mitochondrial-encoded (MitoCarta 2.0) (18), and consequently, many of these regulon members were related not only with the oxidative stress response but also with mitochondrial remodeling (fusion/fission) (Figure 2B). To further strengthen these initial analyses, GSEA showed a robust enrichment for energy metabolism in the coupled group (Figure 2, C and D). The coupled group had an enrichment of genes involved in the TCA cycle ($P = .05$) (Figure 2C) and oxidative phosphorylation ($P = .05$) (Figure 2D), supporting the notion that differences in in vivo mitochondrial coupling are strongly associated with maximal rates of ATP synthesis.

GSEA revealed a highly significant enrichment for FA metabolism genes ($P = .04$) (Figure 2E). Furthermore, IMCL content of the soleus muscle was 35% higher ($P = .03$) (Figure 3A) in coupled vs uncoupled, whereas IMCL content of the tibialis anterior did not differ between groups ($P = .28$) (Figure 3A) in vivo. IMCL content of the VL muscle was 25% higher in the coupled (vs uncoupled) group ($P = .02$) (Figure 3A) ex vivo. GSEA also revealed a significant enrichment for genes related to oxidative stress and UV response ($P = .03$) (Figure 2F).

In vivo mitochondrial coupling is reflective of mitohormesis

The coupled group had elevated mRNA content of nicotinamide phosphoribosyltransferase (*NAMPT*) ($P < .05$) (Figure 4A), which supports the enrichment analyses pointing toward an oxidative stress response (Figure 2) even in the absence of a difference in a marker of the deleterious effects of ROS (eg, lipid peroxidation, 4-HNE;

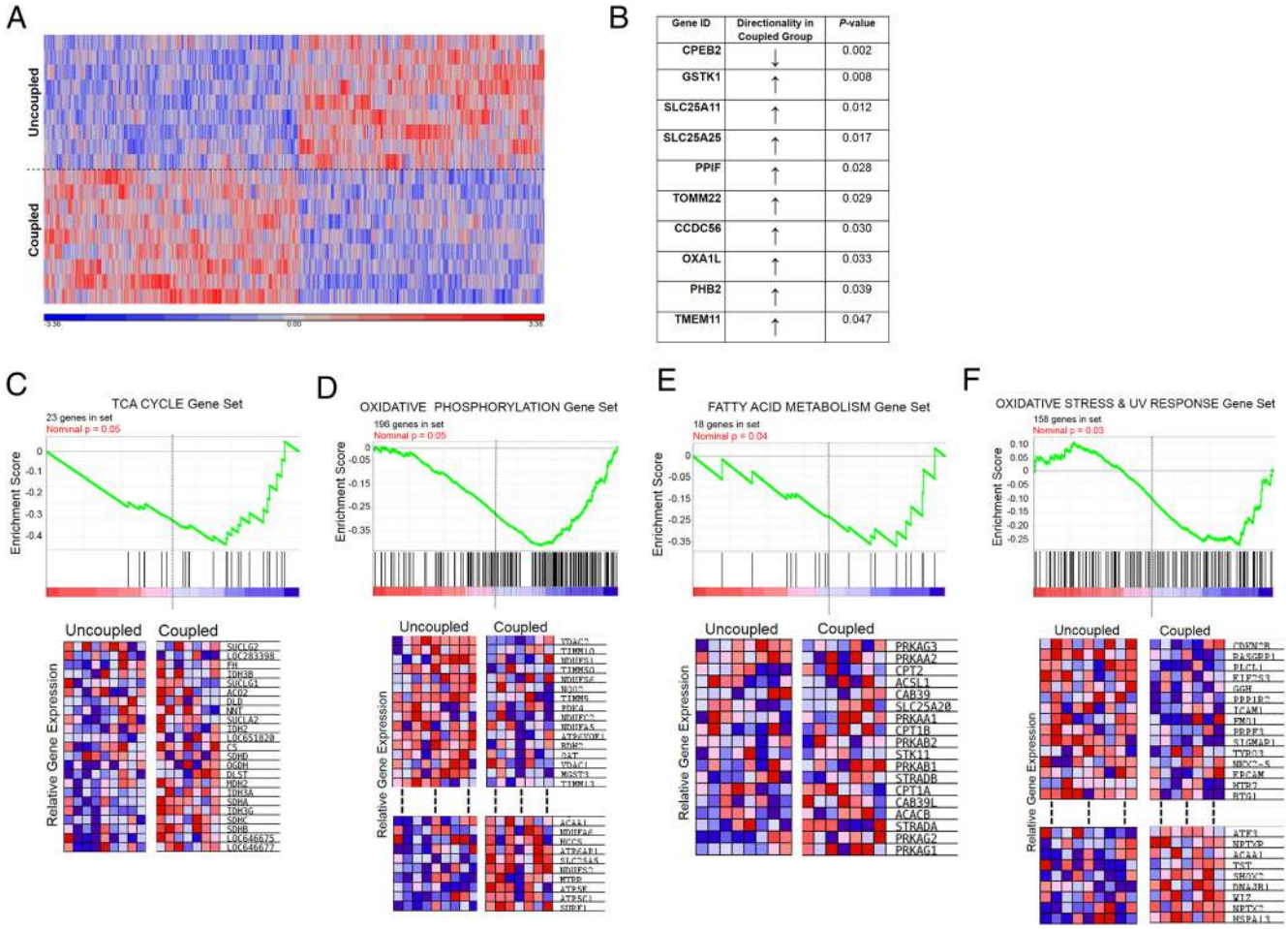

Gene ID	Directionality in Coupled Group	*P*-value
CPEB2	↓	0.002
GSTK1	↑	0.008
SLC25A11	↑	0.012
SLC25A25	↑	0.017
PPIF	↑	0.028
TOMM22	↑	0.029
CCDC56	↑	0.030
OXA1L	↑	0.033
PHB2	↑	0.039
TMEM11	↑	0.047

Figure 2. Higher in vivo mitochondrial coupling reveals a transcriptional signature of mitochondrial remodeling and oxidative stress. Unsupervised cluster analysis of Illumina transcription arrays in muscle tissue mRNA generated a "hit list" of 1805 genes. Each color represents the log2 ratio of the (coupled gene expression to uncoupled gene expression) of a particular gene in each participant. Due to tissue limitations, we used a representative sample of 9 participants per group. Red indicates up-regulation and blue indicates down-regulation. The unadjusted *P* value cutoff was set at 0.05. Each column shows data from a specific gene and each row shows data from a single participant (A). Of the 1805 genes significantly regulated between the 2 groups, 23 regulons were found, each containing hundreds to thousands of genes via a VIPER analysis. Of the 23 total, 1 regulon had the Master Regulator (CPEB2) at its center node with 1005 genes in its regulon. All gene members of the regulon were significantly related to the Master Regulator *CPEB2* ($P < .05$) via corresponding AracNe mutual information/network edge. Each of the 1005 genes were also represented among other regulons. A selected number of these regulon gene members are depicted in the Table. 4% of the genes in this regulon are encoded by mtDNA. Functions were determined with MetaCore and available gene ontology (GO) and shown to be involved in oxidative stress and apoptotic responses, as well as mitochondrial morphogenesis and remodeling (eg, fusion/fission) (B). As a follow-on to these analyses, GSEA of the same transcriptomics dataset from (A) was performed. In the Reactome gene set list, 2 sets were significantly different between groups: TCA cycle and oxidative phosphorylation, which were up-regulated in the coupled group (C and D). In the Hallmark gene set lists, 2 sets were significantly different between groups: FA metabolism and oxidative stress and UV response, which were up-regulated in the coupled group (E and F). The dashed lines in D and F indicate the portions of the heat map that were truncated due to space limitations. SLC25A11, SLC family 25 member 11/mitochondrial 2-oxoglutarate; GSTK1, glutathione S-transferase κ-1; CCDC56, coiled coil domain-containing protein 56/cytochrome c oxidase assembly factor; OXA1L, oxidase (cytochrome c) assembly 1 like; PHB2, prohibitin 2; PPIF, peptidylprolyl isomerase F; SLC25A25, SLC family 25 member 25; TOMM22, translocase of outer mitochondrial membrane protein 22; TMEM11, transmembrane protein 11.

$P = .55$) (Figure 3B). The coupled group tended to have an increased ratio of Uqcrc2 (mtDNA-encoded ETS protein) to solute carrier (SLC)25A4 (nDNA-encoded component of the inner mitochondrial membrane) protein contents (Uqcrc2/SLC25A4, $P = .06$; coupled vs uncoupled group) (Figure 4B). This imbalance is associated with induction of the mitochondrial unfolded protein response (UPR^{mt}), an adaptive and hermetic signaling pathway that repairs and improves mitochondrial function. Protein content of the mitochondrial chaperone HSP60, which is induced during UPR^{mt}, was significantly higher in the coupled group ($P = .004$) (Figure 4C).

Based on our findings here, Figure 5 summarizes our hypothesized view of the complex relationship between the oxidative stress response and mitohormesis as a continuous feedback loop in response to certain stimuli such as exercise (1, 2) and caloric restriction (CR) (25) that can create more tightly coupled mitochondria as a function of

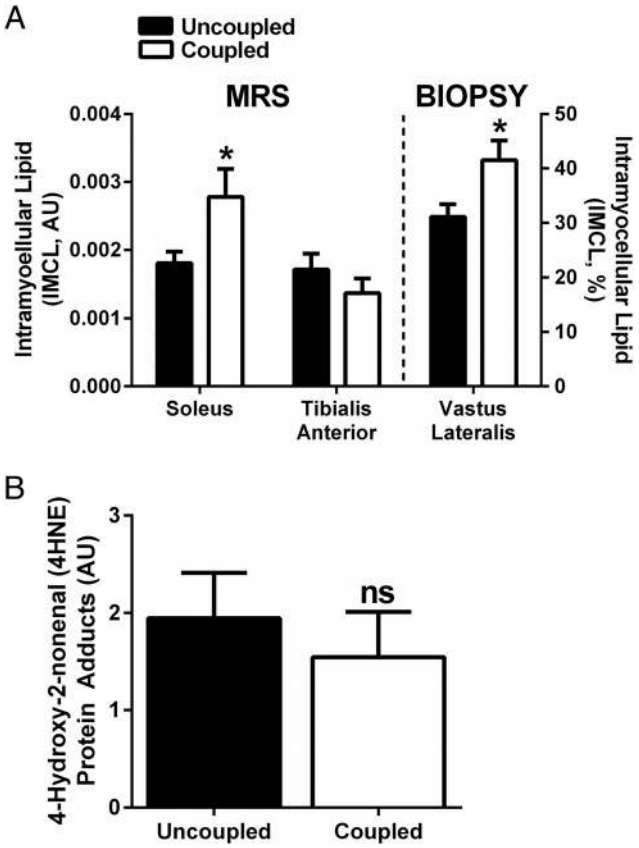

Figure 3. Higher in vivo mitochondrial coupling is associated with elevated myocellular lipid in the absence of lipid peroxidation. In vivo IMCL content was measured by ^{1}H-MRS in both soleus and tibialis anterior muscles relative to water. Areas of interest were expressed in arbitrary units per voxel area relative to internal water (%IMCL = IMCL peak area/water peak area × 100). Tissue IMCL was measured by immunohistochemistry in the VL muscle (from biopsy) using Oil Red O staining (A). 4-HNE protein adducts were quantified by Western blotting in the VL muscle (from biopsy) as a marker of lipid peroxidation (B). All data are expressed as the mean ± SEM. Black bars indicate uncoupled and white bars indicate coupled. For IMCL by ^{1}H-MRS, n = 23 (uncoupled) and n = 21 (coupled); for tissue IMCL, n = 13 (uncoupled) and n = 9 (coupled); for 4-HNE, n = 12 (uncoupled) and n = 12 (coupled) due to tissue limitations. *, $P < .05$; ns, not significant.

time. Our results demonstrate that high muscle mitochondrial coupling is associated with elevated maximal ATP synthesis, muscle lipid content, and expressions of genes related to mitochondrial biogenesis and function, particularly those involved in NAD^+ biosynthesis, the oxidative stress response and mitochondrial remodeling.

Discussion

Athletes have higher in vivo P/O and antioxidant enzyme content compared with their sedentary counterparts (2), suggesting that enhanced mitochondrial coupling may be related to a more effective oxidative stress response that serves as a buffer for ROS production. Although high levels of intracellular ROS trigger detrimental effects on cellular function (26), lower levels of ROS can up-regulate antioxidant enzyme activities and elicit a cytoprotective response. For example, CR-induced increases in lifespan have been linked to increased ROS production (27). Similarly, NAD^+ boosters that improve overall mitochondrial function do so through ROS generation and a mitonuclear protein imbalance that initiates the UPR^{mt} (28). Mitohormesis, a process that engages a nonlinear response to mitochondrial ROS, results in health span-promoting effects when amounts of ROS are low (29). Here, we have demonstrated that in nonobese healthy humans, enhanced muscle mitochondrial coupling is associated with elevated maximal ATP synthesis, muscle lipid content, and expressions of genes related to mitochondrial function, particularly those involved in NAD^+ biosynthesis, the oxidative stress response, and mitochondrial fusion/fission.

ATPmax is associated with P/O in athletes and healthy sedentary individuals (2) and with VO_2peak in older adults (30). We found that higher P/O was associated with higher ATPmax, despite similar VO_2peak in our healthy sedentary adults, suggesting that the observed relationship between P/O and ATPmax may be intrinsic to the mitochondria and not related to whole-body oxygen consumption. However, because P/O and ATPmax were measured at rest and VO_2peak was obtained during an exercise test, it is difficult to conclude. Type I muscle fibers are typically indicative of a highly oxidative phenotype (31). The significantly lower type IIx (glycolytic) fiber content, coupled with significantly higher type IIa (more oxidative) fiber content, in the coupled group suggests a shift towards a more oxidative phenotype and could explain the higher P/O; however, without a concomitant elevation in type I fiber content, fiber composition alone does not account for the differences in muscle P/O between groups. Additionally, mitochondrial content (mtDNA) was similar between the 2 groups, yet mRNA levels of key substrate metabolism genes (*PPARGC1A*, *PPARD*, and *CS*) were significantly higher in the coupled group. Collectively, these results support the notion that in vivo measurements of P/O and ATPmax reflect muscle mitochondrial function rather than fiber type or mitochondrial content at the tissue level or aerobic capacity at the whole-body level.

Studies in mitochondria isolated from human quadriceps muscle indicate that maximal P/O ≈ 2.3–2.5 (32, 33). We have previously demonstrated reduced coupling of the tibialis anterior muscle in vivo in healthy adults (mean P/O = 2.0; range, ~1.0–3.0) (10). Although our observed range of P/O = 0.49–2.17 in the present study corroborates these previous findings, the P/O < 1.22 (uncoupled group) might be indicative of mild uncoupling. UCP3 and ANT1 have prominent roles in mediating uncoupling in

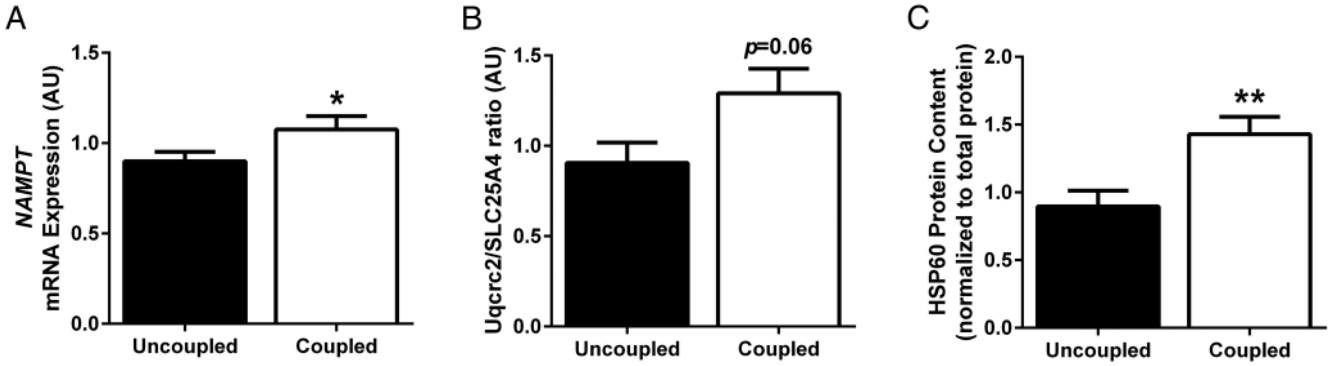

Figure 4. Higher in vivo mitochondrial coupling reveals a novel signature of mitohormesis. mRNA levels of NAMPT (A) and protein levels of mtDNA-encoded Uqcrc2 and nDNA-encoded SLC25A4 (B) and HSP60 (C) are elevated in the coupled group, indicating a mitonuclear imbalance and induction of the UPR^{mt}, which reflect mitohormesis. All data are expressed as the mean ± SEM. Black bars indicate uncoupled and white bars indicate coupled. mtDNA, mtDNA; nDNA, and nDNA; n = 16 (uncoupled) and n = 15 (coupled) due to limited tissue availability; **, $P < .01$; *, $P < .05$.

human and rodent muscles (32, 34). Because we found no differences at the transcript or protein level, it is less likely that uncoupling and elevations in leak-dependent respiration are contributing to the observed differences in mitochondrial function between the coupled and uncoupled groups; however, it is important to note that posttranslational modifications of UCP3 (22) and ANT1 proteins (22), in addition to ANT1 activity itself (6), play an important role in mitochondrial function regardless of mRNA expression or protein levels.

We observed a novel transcriptional profile indicative of elevated oxidative stress response and mitochondrial fusion/fission in the coupled group. An in-depth bioinformatics analysis (Viper) (17) revealed a group of more than 1000 genes ("regulon") with a single "master regulator" (*CPEB2*), a negative regulator of the oxidative stress response, at its node that was significantly lower in the coupled group. *CPEB2* regulates *Hif1a* translation under the direction of another critical oxidative stress sensor, glutathione peroxidase 7 (24). Members of the regulon associated with the oxidative stress response, redox homeostasis (*SLC25A11* and *GSTK1*) and mitochondrial remodeling (*CCDC56*, *OXA1L*, *PHB2*, *PPIF*, *SLC25A25*, *TOMM22*, and *TMEM11*) were significantly higher in the coupled group. GSEA confirmed an enrichment of genes involved in TCA cycle and ETS function and the oxidative stress response.

NAMPT has been implicated in the oxidative stress response induced with CR (35). In addition to mitochondrial function genes (*PPARGC1A*, *PPARD*, and *CS*), expression of *NAMPT* was significantly elevated in individuals with higher P/O. Recent reports show that stimulation of the NAD^+ biosynthesis pathway (via NAMPT) has beneficial effects on mitochondrial function, which supports the enrichment analyses pointing toward an oxidative stress response even in the absence of a difference in a marker of the deleterious effects of ROS (eg, lipid peroxidation, 4-HNE). The concept that sublethal stress can protect against larger subsequent stresses, particularly in mitochondria (mitohormesis) (36), coupled with our transcriptional signature of an oxidative stress response and mitochondrial fusion/fission, encouraged us to examine whether a mitonuclear protein imbalance (a stoichiometric imbalance between mitochondrial proteins encoded by the mtDNA and nDNA) could be related with higher P/O. We showed that a trend for mitonuclear protein imbal-

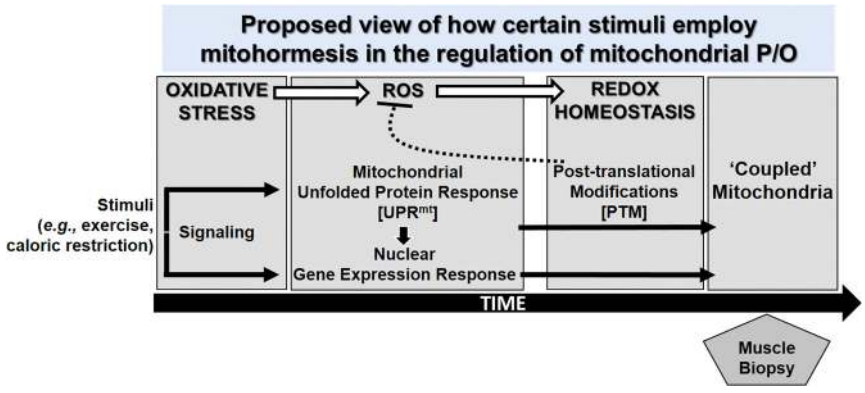

Figure 5. Schematic of a hypothesized redox circuit linking episodic oxidative stress with coupled mitochondria. Proposed model shows the integration of an exercise- or CR-induced oxidative stress signal with both mitochondrial- and nuclear-derived ROS via unfolded protein responses (UPR^{mt}) and gene expression, respectively, and retrograde signaling via posttranslational modifications (PTMs) that feedback to inhibit ROS signaling, providing a mechanism by which redox control processes regulate mitochondrial coupling (eg, mitohormesis) as a function of time. Importantly, the muscle biopsies (and corresponding in vivo measurements) were performed distant in time from the upstream signaling and subsequent nuclear- and mitochondrial-driven responses that lead to coupled mitochondria.

ance and a significant elevation in HSP60 protein indicating UPR^{mt} induction were present in the muscle of the coupled group. A recent report demonstrated that treatment of type 2 diabetes with an NAD^+ precursor (Acipimox) improved muscle mitochondrial function in part through initiation of the UPR^{mt} via a mitonuclear protein imbalance (28).

FAs are a robust substrate for mitochondrial metabolism. We have previously demonstrated that proximity of lipid droplets to the mitochondrion is a critical regulator of muscle FA flux and oxidation (37). In vivo and ex vivo muscle lipid contents were significantly elevated in individuals with higher mitochondrial coupling (P/O), which was supported by GSEA showing a significant enrichment of genes involved in FA metabolism in the coupled group. High levels of muscle lipid content have been reported in individuals with elevated mitochondrial function (14). Ectopic lipid deposition per se is not indicative of pathology, and in our present cohort of healthy nonobese individuals, higher levels of muscle lipid are reflective of higher mitochondrial coupling.

In summary, our results demonstrate that in nonobese healthy humans, enhanced muscle mitochondrial coupling is associated with elevated maximal ATP synthesis, muscle lipid content, and expressions of genes related to mitochondrial function, particularly those involved in NAD^+ biosynthesis, the oxidative stress response, and mitochondrial remodeling (fusion/fission). In the absence of differences in VO_2peak and physical activity-related energy expenditure, our data also suggest that this mitochondrial phenotype is intrinsic rather than extrinsic. Mitohormesis is a potential explanation for the transcriptional signature of an oxidative stress response and mitochondrial remodeling, together with the indication of UPR^{mt}, that we have observed in our cohort of individuals with higher mitochondrial coupling. As put forth in Figure 5, our findings support a working hypothesis that stimuli such as CR and exercise elicit their beneficial effects via inductions of mild metabolic stress and that this occurs presumably through fine tuning of redox circuitry (38) either by signaling through mitochondrial-generated ROS and retrograde signaling via posttranslational modifications (22) or through nuclear-generated ROS signaling and subsequent downstream nuclear signaling (39). Although we have executed all of measurements in the resting state (ie, not following exercise), we have likely captured snapshots of this process whereby we observed coupled mitochondria with elevated oxidative stress yet in the absence of an overt elevation in a marker of the deleterious effects of ROS (eg, lipid peroxidation) (Figure 5B). Moving forward, the potential of having a mitochondrial signature with which individuals can be identified before an intervention (eg, CR, exercise) and used to predict their response (the so-called responders and nonresponders) has significant clinical implications.

Acknowledgments

We thank the study participants, Kori Murray of Pennington Biomedical Research Center for her help with the MRS measurements, Joshua Smith and Milan Srivastava of the Translational Research Institute for Metabolism and Diabetes for their help with Western blotting, and the efforts of the CALERIE data coordinating center (James Rochon, William Krauss, and Manjushri Bhapkah).

Address all correspondence and requests for reprints to: Lauren M. Sparks, PhD, Translational Research Institute for metabolism and Diabetes, Florida Hospital, 301 East Princeton Street, Orlando, FL 32804. E-mail: lauren.sparks@flhosp.org.

Author contributions: L.M.S. analyzed and interpreted the data and wrote the manuscript. A.H., A.E., S.R.C., M.E.G., F.Y., C.S., and H.H.C. assisted during the acquisition, analysis, and interpretation of data and revised the manuscript. L.M.R., K.E.C., M.-E.H., and E.R. contributed to the design of the study, analyzed and interpreted the data, and edited the manuscript. S.R.S. designed the study, analyzed and interpreted the data, and edited the manuscript. All authors approved the final version of the manuscript. L.M.S. and S.R.S. are responsible for the integrity of the work as a whole.

This work was supported by National Institutes of Health Grants R01 AG030226 (to S.R.S.) and R01 AG029914 and U01 AG020478 (to E.R.) and in part by National Institutes of Health Grants P30 DK072476 (Pennington/Louisiana Nutrition and Obesity Research Center) and U54 GM104940 (Louisiana Clinical and Translational Science Center).

Disclosure Summary: The authors have nothing to disclose.

References

1. **Conley KE, Amara CE, Jubrias SA, Marcinek DJ.** Mitochondrial function, fibre types and ageing: new insights from human muscle in vivo. *Exp Physiol*. 2007;92(2):333–339.
2. **Conley KE, Amara CE, Bajpeyi S, et al.** Higher mitochondrial respiration and uncoupling with reduced electron transport chain content in vivo in muscle of sedentary versus active subjects. *J Clin Endocrinol Metab*. 2013;98(1):129–136.
3. **Mason SA, Morrison D, McConell GK, Wadley GD.** Muscle redox signalling pathways in exercise. Role of antioxidants. *Free Radic Biol Med*. 2016;98:29–45.
4. **Seifert EL, Bastianelli M, Aguer C, et al.** Intrinsic aerobic capacity correlates with greater inherent mitochondrial oxidative and H2O2 emission capacities without major shifts in myosin heavy chain isoform. *J Appl Physiol (1985)*. 2012;113(10):1624–1634.
5. **Parker N, Affourtit C, Vidal-Puig A, Brand MD.** Energization-dependent endogenous activation of proton conductance in skeletal muscle mitochondria. *Biochem J*. 2008;412(1):131–139.
6. **Sparks LM, Gemmink A, Phielix E, et al.** ANT1-mediated fatty acid-induced uncoupling as a target for improving myocellular insulin sensitivity. *Diabetologia*. 2016; 59(5):1030–1039.
7. **Ravussin E, Redman LM, Rochon J, et al.** A 2-year randomized controlled trial of human caloric restriction: feasibility and effects on

predictors of health span and longevity. *J Gerontol A Biol Sci Med Sci*. 2015;70(9):1097–1104.
8. **Heilbronn LK, de Jonge L, Frisard MI, et al.** Effect of 6-month calorie restriction on biomarkers of longevity, metabolic adaptation, and oxidative stress in overweight individuals: a randomized controlled trial. *JAMA*. 2006;295(13):1539–1548.
9. **Larson-Meyer DE, Smith SR, Heilbronn LK, et al.** Muscle-associated triglyceride measured by computed tomography and magnetic resonance spectroscopy. *Obesity (Silver Spring)*. 2006;14(1):73–87.
10. **Amara CE, Shankland EG, Jubrias SA, Marcinek DJ, Kushmerick MJ, Conley KE.** Mild mitochondrial uncoupling impacts cellular aging in human muscles in vivo. *Proc Natl Acad Sci USA*. 2007; 104(3):1057–1062.
11. **Jubrias SA, Esselman PC, Price LB, Cress ME, Conley KE.** Large energetic adaptations of elderly muscle to resistance and endurance training. *J Appl Physiol*. 2001;90(5):1663–1670.
12. **Bergstrom J.** Percutaneous needle biopsy of skeletal muscle in physiological and clinical research. *Scand J Clin Lab Invest*. 1975;35(7): 609–616.
13. **Gerrits MF, Ghosh S, Kavaslar N, et al.** Distinct skeletal muscle fiber characteristics and gene expression in diet-sensitive versus diet-resistant obesity. *J Lipid Res*. 2010;51(8):2394–2404.
14. **Phielix E, Meex R, Ouwens DM, et al.** High oxidative capacity due to chronic exercise training attenuates lipid-induced insulin resistance. *Diabetes*. 2012;61(10):2472–2478.
15. **Downey T.** Analysis of a multifactor microarray study using Partek genomics solution. *Methods Enzymol*. 2006;411:256–270.
16. **Margolin AA, Nemenman I, Basso K, et al.** ARACNE: an algorithm for the reconstruction of gene regulatory networks in a mammalian cellular context. *BMC Bioinformatics*. 2006;7(suppl 1):S7.
17. **Lefebvre C, Rajbhandari P, Alvarez MJ, et al.** A human B-cell interactome identifies MYB and FOXM1 as master regulators of proliferation in germinal centers. *Mol Syst Biol*. 2010;6:377.
18. **Calvo SE, Clauser KR, Mootha VK.** MitoCarta2.0: an updated inventory of mammalian mitochondrial proteins. *Nucleic Acids Res*. 2016;44(D1):D1251–D1257.
19. **Subramanian A, Tamayo P, Mootha VK, et al.** Gene set enrichment analysis: a knowledge-based approach for interpreting genome-wide expression profiles. *Proc Natl Acad Sci USA*. 2005;102(43): 15545–15550.
20. **Kuehn H, Liberzon A, Reich M, Mesirov JP.** Using GenePattern for gene expression analysis. *Curr Protoc Bioinformatics*. 2008;Chapter 7:Unit 7 12.
21. **Liberzon A, Birger C, Thorvaldsdóttir H, Ghandi M, Mesirov JP, Tamayo P.** The molecular signatures database (MSigDB) hallmark gene set collection. *Cell Syst*. 201(6)5;1:417–425.
22. **Mailloux RJ, Seifert EL, Bouillaud F, Aguer C, Collins S, Harper ME.** Glutathionylation acts as a control switch for uncoupling proteins UCP2 and UCP3. *J Biol Chem*. 2011;286(24):21865–21875.
23. **Mielke C, Lefort N, McLean CG, et al.** Adenine nucleotide translocase is acetylated in vivo in human muscle: modeling predicts a decreased ADP affinity and altered control of oxidative phosphorylation. *Biochemistry*. 2014;53(23):3817–3829.
24. **Chen PJ, Weng JY, Hsu PH, Shew JY, Huang YS, Lee WH.** NPGPx modulates CPEB2-controlled HIF-1α RNA translation in response to oxidative stress. *Nucleic Acids Res*. 2015;43(19):9393–9404.
25. **Lanza IR, Zabielski P, Klaus KA, et al.** Chronic caloric restriction preserves mitochondrial function in senescence without increasing mitochondrial biogenesis. *Cell Metab*. 2012;16(6):777–788.
26. **Negre-Salvayre A, Auge N, Ayala V, et al.** Pathological aspects of lipid peroxidation. *Free Radic Res*. 2010;44(10):1125–1171.
27. **Ristow M, Zarse K.** How increased oxidative stress promotes longevity and metabolic health: the concept of mitochondrial hormesis (mitohormesis). *Exp Gerontol*. 2010;45(6):410–418.
28. **van de Weijer T, Phielix E, Bilet L, et al.** Evidence for a direct effect of the NAD+ precursor acipimox on muscle mitochondrial function in humans. *Diabetes*. 2015;64(4):1193–1201.
29. **Ristow M, Schmeisser K.** Mitohormesis: promoting health and lifespan by increased levels of reactive oxygen species (ROS). *Dose Response*. 2014;12(2):288–341.
30. **Coen PM, Jubrias SA, Distefano G, et al.** Skeletal muscle mitochondrial energetics are associated with maximal aerobic capacity and walking speed in older adults. *J Gerontol A Biol Sci Med Sci*. 2013; 68(4):447–455.
31. **Dubé JJ, Amati F, Stefanovic-Racic M, Toledo FG, Sauers SE, Goodpaster BH.** Exercise-induced alterations in intramyocellular lipids and insulin resistance: the athlete's paradox revisited. *Am J Physiol Endocrinol Metab*. 2008;294(5):E882–E888.
32. **Brand MD, Pakay JL, Ocloo A, et al.** The basal proton conductance of mitochondria depends on adenine nucleotide translocase content. *Biochem J*. 2005;392(Pt 2):353–362.
33. **Larsen FJ, Schiffer TA, Borniquel S, et al.** Dietary inorganic nitrate improves mitochondrial efficiency in humans. *Cell Metab*. 2011; 13(2):149–159.
34. **Brand MD, Esteves TC.** Physiological functions of the mitochondrial uncoupling proteins UCP2 and UCP3. *Cell Metab*. 2(2)005;2: 85–93.
35. **Song J, Ke SF, Zhou CC, et al.** Nicotinamide phosphoribosyltransferase is required for the calorie restriction-mediated improvements in oxidative stress, mitochondrial biogenesis, and metabolic adaptation. *J Gerontol A Biol Sci Med Sci*. 2014;69(1):44–57.
36. **Ristow M.** Unraveling the truth about antioxidants: mitohormesis explains ROS-induced health benefits. *Nat Med*. 20(7)14;20:709–711.
37. **Bosma M, Minnaard R, Sparks LM, et al.** The lipid droplet coat protein perilipin 5 also localizes to muscle mitochondria. *Histochem Cell Biol*. 2012;137(2):205–216.
38. **Fisher-Wellman KH, Lin CT, Ryan TE, et al.** Pyruvate dehydrogenase complex and nicotinamide nucleotide transhydrogenase constitute an energy-consuming redox circuit. *Biochem J*. 2015;467(2): 271–280.
39. **Smith SR, Bai F, Charbonneau C, Janderová L, Argyropoulos G.** A promoter genotype and oxidative stress potentially link resistin to human insulin resistance. *Diabetes*. 2003;52(7):1611–1618.